Available online at www.sciencedirect.com
ScienceDirect
Journal of Computational Physics 227 (2007) 1340–1352
JOURNAL OF COMPUTATIONAL PHYSICS
www.elsevier.com/locate/jcp

Multi-scale plasma simulation by the interlocking of magnetohydrodynamic model and particle-in-cell kinetic model

Tooru Sugiyama *, Kanya Kusano

The Earth Simulator Center, Japan Agency for Marine-Earth Science and Technology, 3173-25 Showa-machi, Kanazawa-ku Yokohama Kanagawa 236-0001, Japan

Received 28 December 2006; received in revised form 27 July 2007; accepted 4 September 2007
Available online 25 September 2007

Abstract

Many kinds of simulation models have been developed to understand the complex plasma systems. However, these simulation models have been separately performed because the fundamental assumption of each model is different and restricts the physical processes in each spatial and temporal scales. On the other hand, it is well known that the interactions among the multiple scales may play crucial roles in the plasma phenomena (e.g. magnetic reconnection, collisionless shock), where the kinetic processes in the micro-scale may interact with the global structure in the fluid dynamics. To take self-consistently into account such multi-scale phenomena, we have developed a new simulation model by directly interlocking the fluid simulation of the magnetohyrdodynamics (MHD) model and the kinetic simulation of the particle-in-cell (PIC) model. The PIC domain is embedded in a small part of MHD domain. The both simulations are performed simultaneously in each domain and the bounded data are frequently exchanged each other to keep the consistency between the models. We have applied our new interlocked simulation to Alfvén wave propagation problem as a benchmark test and confirmed that the waves can propagate smoothly through the boundaries of each domain.

Keywords: Multi-scale; Interlocked simulation; MHD; PIC; Plasma

1. Introduction

Plasma consists essentially of a multi-scale system, that is, various structures and waves are spontaneously formed and excited in widely different scales. The hierarchy of spatial and temporal structure is attributed to the kinetic of particles and the fluid dynamics. Therefore, to capture accurately the property in each scale, numerical plasma simulation has to be performed by an appropriate model. Magneteohydrodynamic (MHD) simulation is one of the most widely utilized tools in plasma research, and it has given substantial contribution to the study of global scale dynamics in space, astrophysical, and experimental plasmas.

* Corresponding author.
E-mail address: tsugi@jamstec.go.jp (T. Sugiyama).

0021-9991/$ - see front matter
doi:10.1016/j.jcp.2007.09.011

The MHD equation is derived from the approximation to large scales in space and time, so that it cannot deal with any kinetic process. On the other hand, the particle-in-cell (PIC), Vlasov and Fokker–Planck simulations are performed in order to handle the micro-scale processes. Since these kinetic simulations essentially contain any plasma processes in their system, the system size is severely restricted in small and short range. Therefore, we have used some idealized (and sometimes impractical) settings for the initial and boundary conditions.

These simulation models in macro- and micro-scales have been separately developed so far. This is because the approximation in fundamental theory in each scale is restricted to specific scale. However, the mutual interaction between the macro-scale dynamics and the micro-scale kinetics plays important roles for various multi-scale plasma phenomena. For instance, the non-gyrotropic particle orbit and the micro-scale instability growing on magnetic neutral lines are widely believed to play crucial roles for the creation of electric field, which drives magnetic reconnection on a thin current sheet [2]. Nevertheless, since there is no adequate method to treat the micro-scale kinetics in the macro-scale system, we have had to treat all the microscopic processes as an artificial model parameter so-called ''anomalous resistivity'' in the large scale MHD simulation. Particle acceleration on large scale collisionless shocks is also the typical multi-scale plasma phenomena, in which reflected and accelerated particles may modify the large scale plasma flow.

Hence, a new methodology to connect consistently the dynamics of the macro-scale and micro-scale is greatly required to be developed. Once this type of method is established, it could help our understanding of complicated plasma processes, and may improve the predictability of the processes. The multi-scale simulation is an issue not only in plasma physics but also in any research fields of sciences and technologies, and the new algorithm and the mathematical framework are demanded to overcome the challenging problems for interconnecting physical processes in vastly different scales. The objective of this paper is to propose a new type of multi-scale plasma simulation algorithm, whereby the mutual interaction between large scale MHD process and micro-scale plasma kinetics is able to be taken into account directly. The strategy in our model is that, only in a limited region where the micro-process is crucial for macro-scale dynamics, the plasma kinetics are calculated with keeping the consistency with the large scale dynamics. In order to accomplish the consistency, we have developed the way to connect the MHD simulation and the kinetic simulation. This new model is an application of the macro–micro interlocked (MMI) simulation which has been recently proposed by [4], for plasma.

In this paper, we adopt the particle-in-cell (PIC) model for the kinetic simulation, and the conventional finite difference method for the MHD simulation, respectively. Therefore, our MHD and PIC interlocked model is resembled to the hybrid continuum-atomistic simulation, which is quickly grown for the study of multi-scale hydrodynamics. For instance, [7] proposed the connection of the conventional fluid model and the particle-based Direct Simulation Monte–Carlo (DSMC) model. However, we should mention the peculiarity in plasma physics in contrast to the hydrodynamics simulations. Since the several characteristics contained in the particle-based (PIC) model are negated in the continuum (MHD) model, some sophisticated filter, which can pass only the proper components for each the macro- and micro-scale models, has to be developed. Therefore, the method proposed here is not a simple application of the hydrodynamic connection model.

This paper is organized as follows: In Section 2, the simulation models are described both for the MHD and the kinetic simulation, and then, the interlocking procedure is explained both for the spatial and temporal connections, respectively. In Section 3, the interlocked model are examined based on the benchmark test for the Alfvén wave propagation problem. Finally, the prospects of the new model are discussed in Section 4.

2. Simulation model

The basic configuration of our MMI plasma simulation is schematically illustrated in Fig. 1. The system consists of two kinds of bounded areas, and in each area the MHD and PIC simulations are performed, respectively. PIC simulations are embedded in the MHD simulation, and the mutual interactions are managed through the boundary among the MHD and PIC domains. The main advantage of our MMI plasma simulation is that both the MHD and PIC simulations are performed simultaneously and the kinetic effects obtained from the PIC domain are self-consistently included in the MHD domain. Therefore a spontaneous data exchange between these two domains through the boundary has great meaning. Otherwise, the results from the PIC domains are included as only parameters as is in conventional ways where the PIC simulations

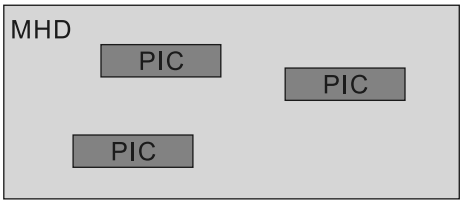

Fig. 1. A schematic illustration of the MHD and PIC interlocked simulation. PIC domains are embedded in MHD domain. MHD simulation handles the whole system, and PIC simulations treat microscopic processes only in the area where the kinetics is necessary to be considered.

and the MHD simulations are separately performed with some idealize boundary conditions, e.g. constant or stationary conditions, and uniform, periodic, mirror, or rigid wall conditions. In this section, we describe how the PIC and MHD domains are associated and connected each other in the points of temporal and spatial directions.

The following set of ideal MHD equations

$$\frac{\partial \rho}{\partial t} = -\nabla \cdot (\rho \boldsymbol{V})$$
$$\frac{\partial \boldsymbol{V}}{\partial t} = -(\boldsymbol{V} \cdot \nabla)\boldsymbol{V} + \frac{1}{\rho}(\nabla P + \boldsymbol{J}_{\mathrm{m}} \times \boldsymbol{B}_{\mathrm{m}})$$
$$\frac{\partial P}{\partial t} = -(\boldsymbol{V} \cdot \nabla)P + \gamma P \nabla P$$
$$\frac{\partial \boldsymbol{B}_{\mathrm{m}}}{\partial t} = \nabla \times \boldsymbol{E}_{\mathrm{m}}$$
$$\boldsymbol{E}_{\mathrm{m}} = -\boldsymbol{V} \times \boldsymbol{B}_{\mathrm{m}}$$
$$\boldsymbol{J}_{\mathrm{m}} = \frac{1}{\mu_0} \nabla \times \boldsymbol{B}_{\mathrm{m}}$$

is used for the MHD simulation, and the full set of equations

$$\frac{\mathrm{d}\boldsymbol{r}^{\#}}{\mathrm{d}t} = \boldsymbol{v}^{\#}$$
$$\frac{\mathrm{d}\boldsymbol{v}^{\#}}{\mathrm{d}t} = \frac{q^{\#}}{m^{\#}}(\boldsymbol{E}_{\mathrm{p}} + \boldsymbol{v}^{\#} \times \boldsymbol{B}_{\mathrm{p}})$$
$$\boldsymbol{J}_{\mathrm{p}} = \sum_{\#} (q\boldsymbol{v})^{\#}$$
$$\frac{\partial \boldsymbol{B}_{\mathrm{p}}}{\partial t} = -\nabla \times \boldsymbol{E}_{\mathrm{p}}$$
$$\frac{\partial \boldsymbol{E}_{\mathrm{p}}}{\partial t} = c^2 \nabla \times \boldsymbol{B}_{\mathrm{p}} - \frac{1}{\varepsilon_0}\boldsymbol{J}_{\mathrm{p}}$$

is used for PIC simulation. The variables are described in conventional format, e.g. ρ is the plasma mass density. The subscription m and p mean the values in MHD and PIC simulations, respectively. The superscription # means the value assigned on individual super-particle in the PIC simulation.

The equation set of PIC simulation has a set of characterized length, time and speed, those are Debye length, the inverse of electron cyclotron frequency, and the speed of light. On the other hand, the set of MHD equations does not have any characteristic length and time but Alfvén speed. Therefore, the spatial and temporal grid width of $\mathrm{d}x$ and $\mathrm{d}t$ are not limited by physical parameters but adopted as arbitrary parameters in the MHD model. We define the ratio of the discretized scales between MHD and PIC as

$$R_x = \mathrm{d}x_{\mathrm{m}}/\mathrm{d}x_{\mathrm{p}},$$
$$R_t = \mathrm{d}t_{\mathrm{m}}/\mathrm{d}t_{\mathrm{p}},$$

where $\mathrm{d}x_\mathrm{p}$ ($\mathrm{d}x_\mathrm{m}$) and $\mathrm{d}t_\mathrm{p}$ ($\mathrm{d}t_\mathrm{m}$) are the spatial and temporal grid width of PIC (MHD), respectively. Since MHD may handle much larger scale, these ratio of R_x, R_t are greater than unity.

2.1. Connection in space

The data exchange is accomplished by the following procedures; (1) the boundary conditions of PIC simulation are determined by the results from the surrounding MHD simulation, and (2) the field data in the PIC domain are sent to MHD. Those are schematically illustrated in Fig. 2a. The overlapped three rectangles in the second panel from top, show the simulation domains of each model. MHD simulation is performed in the whole region of a system (open rectangle area), and PIC simulation is performed in the light and dark-gray shaded area. Note that only one PIC simulation is performed and there is no boundary between light- and dark-gray shaded areas. The difference between light- and dark-gray shaded areas is shown later.

In the PIC simulation, the field data obtained from the surrounding MHD domain are utilized to set the boundary conditions on the lines between open and light-gray shaded area. The conditions are renewed every time step to reflect the results from the MHD simulation. Those conditions are for the particle velocity distribution function and the magnetic- and electric field. The particle velocity distributions for the injecting particles are calculated by using the density, total pressure, bulk velocity, and current density of the MHD simulation. Based on the assumption of local thermal equilibrium, the velocity distribution of the injecting particles has a (shifted-) Maxwell distribution with the same density of the ions and the electrons. The bulk velocity difference between ions and electrons makes current. Then we have,

$$
\begin{aligned}
n_{e\mathrm{p}} &= n_{i\mathrm{p}} = N_\mathrm{m} \\
v_{th,i\mathrm{p}} &= \sqrt{\frac{P_\mathrm{r}}{1+P_\mathrm{r}} P_\mathrm{m} \frac{1}{M_\mathrm{i}}} \\
v_{th,e\mathrm{p}} &= \sqrt{\frac{1}{1+P_\mathrm{r}} P_\mathrm{m} \frac{1}{M_\mathrm{e}}} \\
\boldsymbol{v}_{i\mathrm{p}} &= \boldsymbol{V}_\mathrm{m} \\
\boldsymbol{v}_{e\mathrm{p}} &= \boldsymbol{V}_\mathrm{m} - \frac{\boldsymbol{J}_\mathrm{m}}{N_\mathrm{m} e}
\end{aligned}
$$

where P_r is the pressure ratio between ion and electron as a parameter, and M_i and M_e are ion and electron mass, respectively. We set the shifted-Maxwell velocity distribution every time step of PIC model. A fraction of these particles is injected into the PIC domain [1]. The ejecting particles across the boundary from PIC to MHD are put out of the calculation. Consequently, PIC simulations can be performed under the physical boundary conditions obtained consistently from the MHD simulation. Note that the number of particles in PIC simulations is not constant by a net of the injecting and ejecting particles, and the overall charge in PIC domain does not keep the neutrality.

Fig. 2. (a) Spatial connection method between MHD and PIC domains is schematically illustrated. From top to bottom, the spatial weighting function $W(x)$, the domain decomposition of MHD and PIC simulations, and the field mixing procedure are shown. The area of the MHD and PIC simulations are domain decomposed, and PIC simulation is performed in the dark- and light-gray shaded area, and MHD simulation is performed whole region of the system (open rectangle). The field data of the current density and electric field obtained in the MHD simulations are mixed or replaced by the data from PIC simulation. The weighting function for mixing is $W(x)$ plotted in the top. Before mixing process, the data obtained from PIC simulations are averaged in space and in time in every R_x and R_t, that is, corresponding grid width of MHD simulation, then we have the averaged data of $\overline{\overline{E_\mathrm{p}}}$ and $\overline{\overline{J_\mathrm{p}}}$. The averaged data are mixed with the data of MHD ($\boldsymbol{E}_\mathrm{m}$ and $\boldsymbol{J}_\mathrm{m}$), then we have mixed data of $\boldsymbol{E}_\mathrm{mix}$ and $\boldsymbol{J}_\mathrm{mix}$. The mixing is performed only in the light-gray shaded area. In the dark shaded area, MHD results are replaced by the PIC results. (b) Time sequence of the MHD and PIC interlocked simulation. While the time step is advanced from $T = t$ to $T = t + \mathrm{d}t_\mathrm{m}$, field values are advanced twice by using MHD model (MHD-P:Predictor phase and MHD-C:Corrector phase) and once by PIC model. First, the MHD variables are advanced from $T = t$ to $T = t + \mathrm{d}t_\mathrm{m}$ by the full set of the MHD equations, noted MHD-P. The results of MHD-P are sent to PIC. In the PIC simulation, variables are time advanced by using the temporal boundary condition at $T = t$ and $T = t + \mathrm{d}t_\mathrm{m}$. Then the time-averaged data of $\boldsymbol{E}$ and $\boldsymbol{J}$ are sent to MHD and spatially mixed. Finally the MHD variables are re-advanced from $T = t$ to $T = t + \mathrm{d}t_\mathrm{m}$ by using $\boldsymbol{E}_\mathrm{mix}$ and $\boldsymbol{J}_\mathrm{mix}$ instead of the Ohm's law and Ampère law.

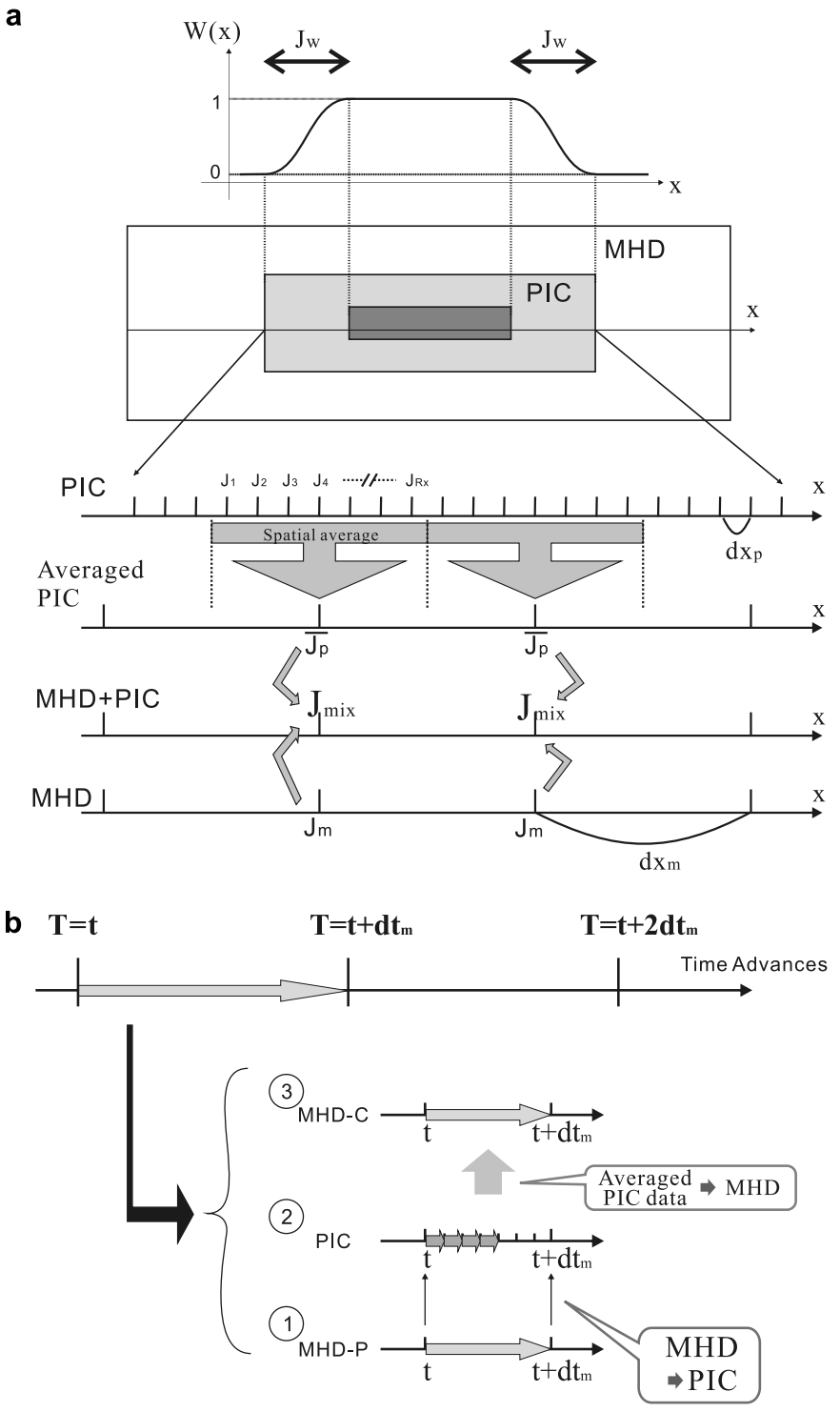

The data transmission from PIC model to MHD model is carried out by the following procedure. Since the spatial and temporal characteristic sizes in PIC simulation are smaller and shorter than those in the MHD simulation, the higher frequency or shorter wave-length waves (e.g. whistler wave) than MHD waves are naturally

contained in the PIC domain. These waves are directly injected into the MHD area through the boundary if the data of PIC and MHD are simply connected. These waves are not resolved in the MHD area because these are not normal mode waves in the MHD equations. It becomes, indeed, an unphysical noise in the MHD system. Only the MHD mode of the low-frequency waves should propagate from PIC to MHD domain. For this purpose, we need some filter which can pass only the low-frequency waves (low-pass filter). In the present interlocked stimulations, the field data of $\boldsymbol{E}_\mathrm{p}$ and $\boldsymbol{J}_\mathrm{p}$ in the PIC domain are averaged in every R_x grids, that is, in the width of MHD grid. Then we have the spatially averaged data $\overline{\boldsymbol{E}_\mathrm{p}}$ and $\overline{\boldsymbol{J}_\mathrm{p}}$, where the shorter wave-length waves than the MHD grid width are filtered out. (See illustrations below the rectangles in Fig. 2a)

The MHD approximation is applicable only for the low-frequency and long-wave-length waves, then the electric field is given by the generalized Ohm's law where the electron inertia, the Hall term, and the electron pressure term are neglected. On the other hand, in the PIC model, the electric field is derived directly from the Maxwell equation where all kinds of kinetics are included. Therefore, it is a natural way to replace the generalized Ohm's law with the results from PIC model when one takes the kinetic effects into the MHD model. These processes are performed by the following procedures. First, we make the averaged data in space noted above, and in time explained in detail later in Section 2.2, those are $\overline{\overline{\boldsymbol{E}_\mathrm{p}}}$ and $\overline{\overline{\boldsymbol{J}_\mathrm{p}}}$. Next, the data of $\overline{\overline{\boldsymbol{E}_\mathrm{p}}}$ and $\overline{\overline{\boldsymbol{J}_\mathrm{p}}}$ are mixed with the MHD results of $\boldsymbol{E}_\mathrm{m}$ and $\boldsymbol{J}_\mathrm{m}$ on the corresponding grids. The weighting function $W(x)$ plotted in the top of Fig. 2a, is applied for mixing as

$$\boldsymbol{E}_\mathrm{mix}(x) = W(x)\overline{\overline{\boldsymbol{E}_\mathrm{p}(x)}} + [1 - W(x)]\boldsymbol{E}_\mathrm{m}(x),$$

$$\boldsymbol{J}_\mathrm{mix}(x) = W(x)\overline{\overline{\boldsymbol{J}_\mathrm{p}(x)}} + [1 - W(x)]\boldsymbol{J}_\mathrm{m}(x).$$

For $W(x)$ we use a square of sine/cosine function in the light-gray shaded area and a constant function in the dark-gray shaded area in Fig. 2a. Finally, $\boldsymbol{E}_\mathrm{mix}$ and $\boldsymbol{J}_\mathrm{mix}$ are used in place of $\boldsymbol{E}_\mathrm{m}$ and $\boldsymbol{J}_\mathrm{m}$ for the MHD equations. In the dark-gray shaded area, the mixing process simply means the replacing $\boldsymbol{E}_\mathrm{m}$ and $\boldsymbol{J}_\mathrm{m}$ to $\overline{\overline{\boldsymbol{E}_\mathrm{p}}}$ and $\overline{\overline{\boldsymbol{J}_\mathrm{p}}}$ because the weighting function is unity. In the transition zone (denoted by light-gray shaded area), both PIC and MHD results are mixed and the kinetic effects are partially taken into account. Resultantly, in the light-gray shaded area, the short wave-length waves are smoothly diminished and mainly the long wave-length components are preferentially sent to the MHD domain. The remained variables of the density, velocity and pressure are directly connected with the velocity moment of particles on the corresponding grid without the above mixing procedure.

In order to realize a non-reflecting open boundary of PIC simulation, we have also adopted the absorbing/damping region at the end of the system where the fluctuations of the electric and magnetic field are reduced [6]. Note that we have not adopt the retarding boundary condition, but introduced the damping region in the whole area of the transition zone plotted by the light-gray shaded area in Fig. 2a.

2.2. Connection in time

To perform the interlocked simulation, it is necessary that the data of both MHD and PIC simulations are exchanged frequently. It is determined as an adjustable parameter how frequently the data are exchanged, then, we have introduced the most frequent connection that the exchange is carried out at every MHD time step. Fig. 2b shows a schematic illustration of the time sequence for the interlocked model. We call the algorithm as "predictor-corrector", where the time is advanced twice in the same MHD time step by predictor phase and corrector phase, respectively. The time step chart consists of the followings three steps. First, the MHD variables are advanced from $T = t$ to $T = t + \mathrm{d}t_\mathrm{m}$ by the full set of the MHD equations. This is the predictor phase as noted MHD-P in Fig. 2. Then, the data both at $T = t$ and $T = t + \mathrm{d}t_\mathrm{m}$ are sent to PIC. Next, the PIC variables (i.e. field and particles) are advanced from $T = t$ to $T = t + \mathrm{d}t_\mathrm{m}$ by using the temporal boundary conditions obtained from MHD simulation at $T = t$ and $T = t + \mathrm{d}t_\mathrm{m}$ and spatial boundary conditions noted in Section 2.1. The temporal boundary conditions are interpolated on every time step in the PIC simulation. While the PIC model is time advanced from $T = t$ and $T = t + \mathrm{d}t_\mathrm{m}$, the data of the electric field ($\boldsymbol{E}_\mathrm{p}$) and the current density ($\boldsymbol{J}_\mathrm{p}$) are time-averaged. This is also the low-pass filter as noted in Section 2.1. Therefore, we calculate the spatially and temporally averaged data of $\overline{\overline{\boldsymbol{E}_\mathrm{p}}}$ and $\overline{\overline{\boldsymbol{J}_\mathrm{p}}}$. The averaged data are sent to MHD and mixed with MHD results. Finally, we again advance the MHD variables from $T = t$ to

$T = t + \mathrm{d}t_\mathrm{m}$ by using the mixed field data of $\boldsymbol{E}_\mathrm{mix}$ and $\boldsymbol{J}_\mathrm{mix}$ instead of the generalized Ohm's law and Ampère's law. This is the corrector phase as noted MHD-C in Fig. 2b. The present interlocked simulation is carried out with this ''predictor-corrector'' algorithm.

3. Test on Alfvén wave propagation

The interlocked simulations between PIC and MHD are applied on the Alfvén wave propagation. The simulations are one-dimensional in space of X-axis, but fully three-dimensional in velocity. In the present PIC simulation code, we have used Kyoto university one-dimensional ElectroMagnetic Particle cOde (KEMPO1) [3]. Hereafter, magnetic field and density are normalized by the background value B_0 and N_0. Velocity, time, and length, are normalized by the Alfvén velocity V_A, the inverse of proton gyro-frequency Ω_{ci}^{-1}, and the ion inertia length $\lambda_i \equiv V_\mathrm{A}/\Omega_{ci}$. The background magnetic field has only X-component and small-amplitude, left-hand circularly polarized Alfvén waves are superposed in Y and Z-components of the magnetic field and velocity, as the wave propagates to positive direction in X-axis. The amplitude and wave-length of the superposed field perturbations are 0.01 and ~105 in the normalized unit. The MHD simulation covers in the range of $X = 0$ to 524.3 with a periodic boundary condition. The embedded PIC simulation is calculated in the range of $X = 249$ to 275. The grid-cell size $\mathrm{d}x_\mathrm{p}$ and the time step size $\mathrm{d}t_\mathrm{p}$ are 1.6×10^{-3} and 3.8×10^{-5}, respectively. The mass ratio between electrons and ions is 400 and the plasma beta is 0.01 for electrons and ions. Initially 100 particles per grid-cell are used for the unit density in the background distribution for each electrons and ions. This number is typical in performing the PIC model. The ratios of the length and time steps between MHD and PIC are $R_\mathrm{t} = 64$ and $R_x = 64$. We define the Alfvén transit time τ_A as the period of the perturbation to propagate over the wave-length of 105 λ_i, which corresponds to ~2.76 million steps in PIC simulation.

Fig. 3a shows the wave form at $T = 0.11\tau_\mathrm{A}$ with an initial wave form at $T = 0$ (green curve). Plotted curves are the Y-component of magnetic field. The blue solid curves show the result from MHD simulation, and the red curves show the results from PIC simulation. The red curved area covers the light- and dark-gray shaded area in Fig. 2a. By comparing the global shape of the blue and green curves, we can see that the Alfvén waves propagate with keeping its wave form and amplitude. The Alfvén waves are scarcely modified in the area of PIC domain and the waves propagate with the Alfvén speed. The expanded plots of the waves around the PIC area are shown at $T = 0.05\tau_\mathrm{A}$ (Panel b) and 0.11 τ_A (Panel c). At the edge of the PIC domain, the amplitude is diminished by the interlocking algorithm of the mixing procedure. The field values automatically approach to the MHD values, and PIC and MHD simulations are smoothly connected each other. In the PIC domain, short wave-length (high-frequency) waves are observed in addition to the global Alfvén wave. The amplitude is still smaller than the amplitude of the background Alfvén wave. Those are normal mode waves in the PIC simulations (e.g. whistler waves) which are not represented in the MHD simulations.

To check the wave properties in both MHD and PIC area, these waves are decomposed into wave number (k) and frequency (Ω) space by using FFT method. Fig. 4 shows the $\Omega - k$ diagram for the different three area. Panel (a) shows the results sampled in the PIC area. Panels (b) and (c) are sampled in the MHD area of the left and right side of the PIC area, respectively. The short wave-length, high-frequency waves observed in Fig. 3 are shown on the branch of the Whistler wave noted by the black solid curve in Fig. 4a. As noted above section, these high-frequency waves should be absorbed by the averaging and mixing procedures noted in Section 2.1, because these waves are unphysical mode in MHD simulation. In our model, the connection procedure well works as shown in Panels (b) and (c). Even though the Whistler waves are excited as clearly observed in Panel (a), only the imposed Alfvén waves are observed in Panels (b) and (c). Indeed, only a small fraction of wave power of the short wave-length wave is emitted into the MHD domain which are observed in the wave form plotted in Fig. 3b and c and in spectra plotted in Fig. 4b and c on the Alfvén mode branch. The amplitude of the fluctuations/waves is small enough for Alfvén wave propagation process.

4. Summary and discussion

We have explained the algorithm of the MHD and PIC interlocked simulation. This new algorithm is applied to Alfvén wave propagation problem in one-dimensional system. The wave smoothly propagates from MHD into PIC domain and ejected again into MHD. While the wave is propagating in the PIC domain, the

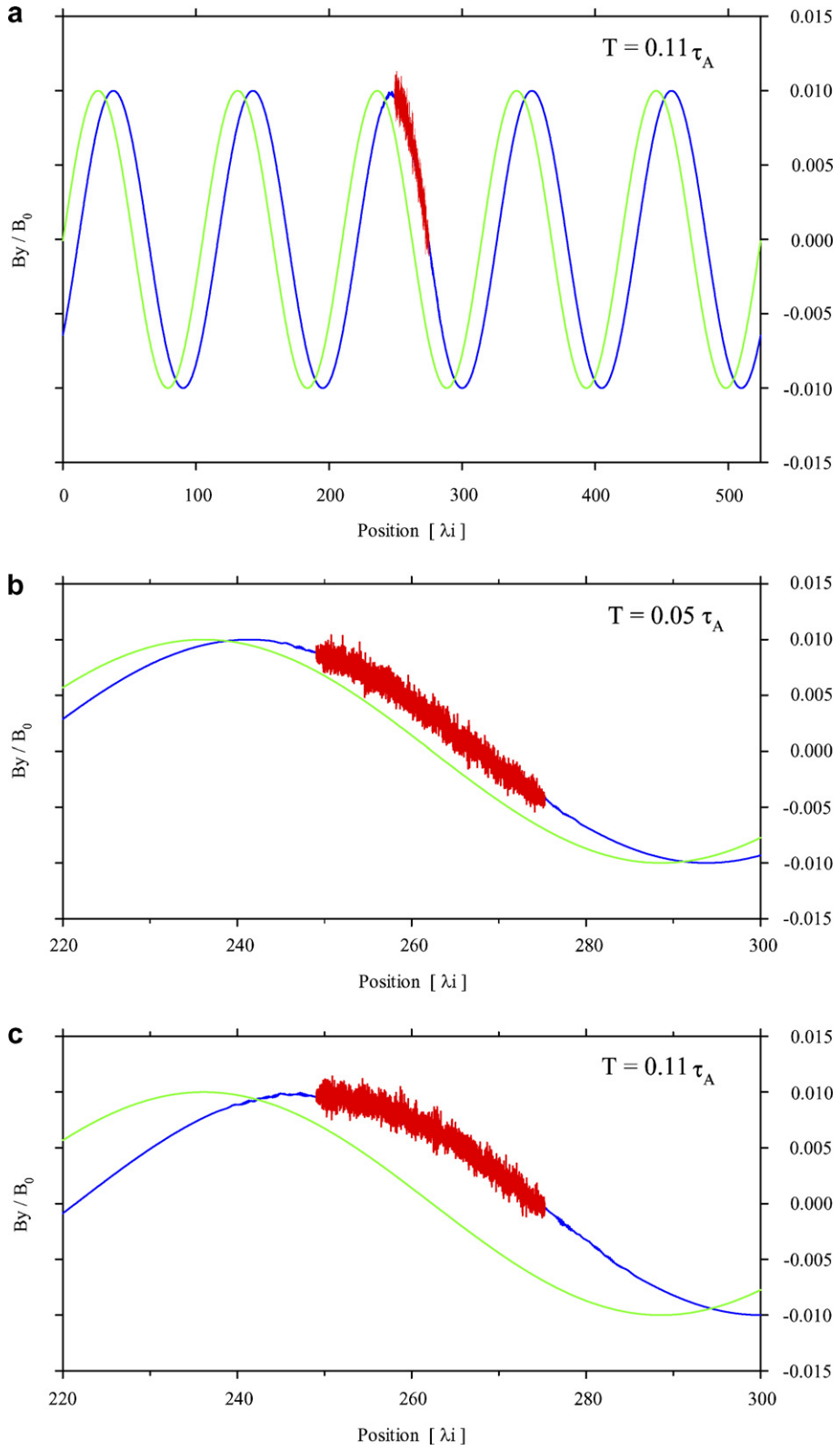
a
T = 0.11 τA
By / B0
0.015
0.010
0.005
0.000
-0.005
-0.010
-0.015
0
100
200
300
400
500
Position [λi]
b
T = 0.05 τA
By / B0
220
240
260
280
300
Position [λi]
c
T = 0.11 τA
By / B0
220
240
260
280
300
Position [λi]

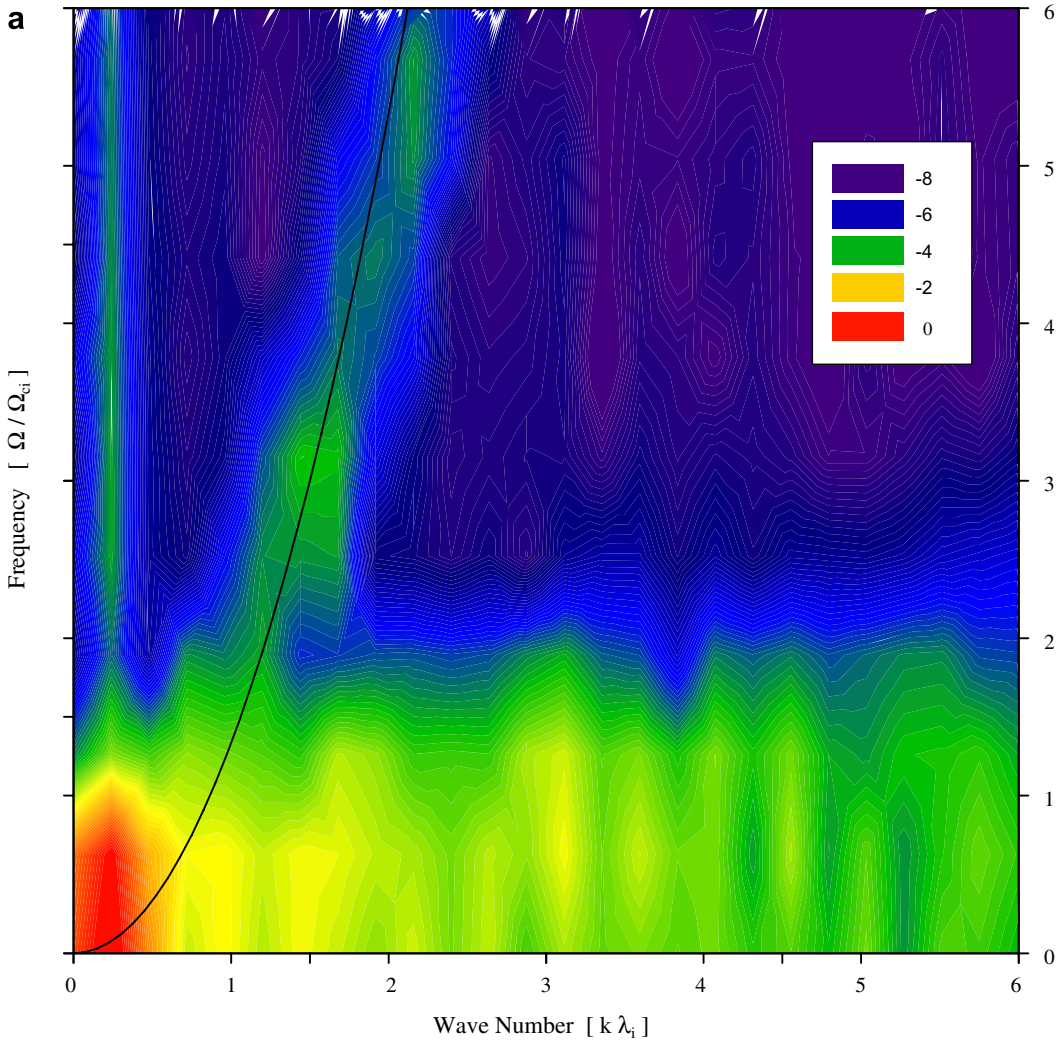

Fig. 4. Ω–k diagram sampled in the different three area are plotted with color contour in logarithm unit. Panel (a) shows the results sampled in the PIC domain. Black curve shows the branch of the Whistler wave. The short wave-length, high frequent waves observed in Fig. 3 are, indeed, the Whistler wave. Panels (b) and (c) are sampled in the MHD domain of the left and right side of the PIC domain, respectively. Even though the high-frequency waves are excited in the PIC domain, only the original MHD mode waves are clearly observed in the MHD domain.

wave almost keeps its form and amplitude, even though some high-frequency fluctuations are excited. Their power is smaller than that of the Alfvén wave.

Here, we discuss about a wave shift illustrated in Fig. 5. In the parallel direction of the magnetic field, the wave dispersion relation in the low-frequency range ($<\Omega_{ci}$) is decomposed into two branches, those are, Whistler wave (R-mode wave) and Ion cyclotron wave (L-mode wave) which propagate with different velocity. This

Fig. 3. Wave form at time 0.11 τ_A (Panel a) and two expanded plots around the PIC domain at 0.05 τ_A (Panel b) and 0.11 τ_A (Panel c), where τ_A is an Alfvén transit time (see text). Plotted are Y-component of the magnetic field. Green curve in each panel shows an initial wave form of the left-hand circularly polarized Alfvén waves. The wave-length and amplitude are ~105 and 0.01 in the normalized unit. MHD simulations are performed in the full region of the system whose length is ~524.3 with a periodic boundary condition. The results are plotted by blue curves. PIC simulation is performed in the range of 249 to 275 and results are plotted by red curves. As time elapses, the Alfvén wave smoothly propagates to positive direction in X-axis with keeping its wave form and amplitude.

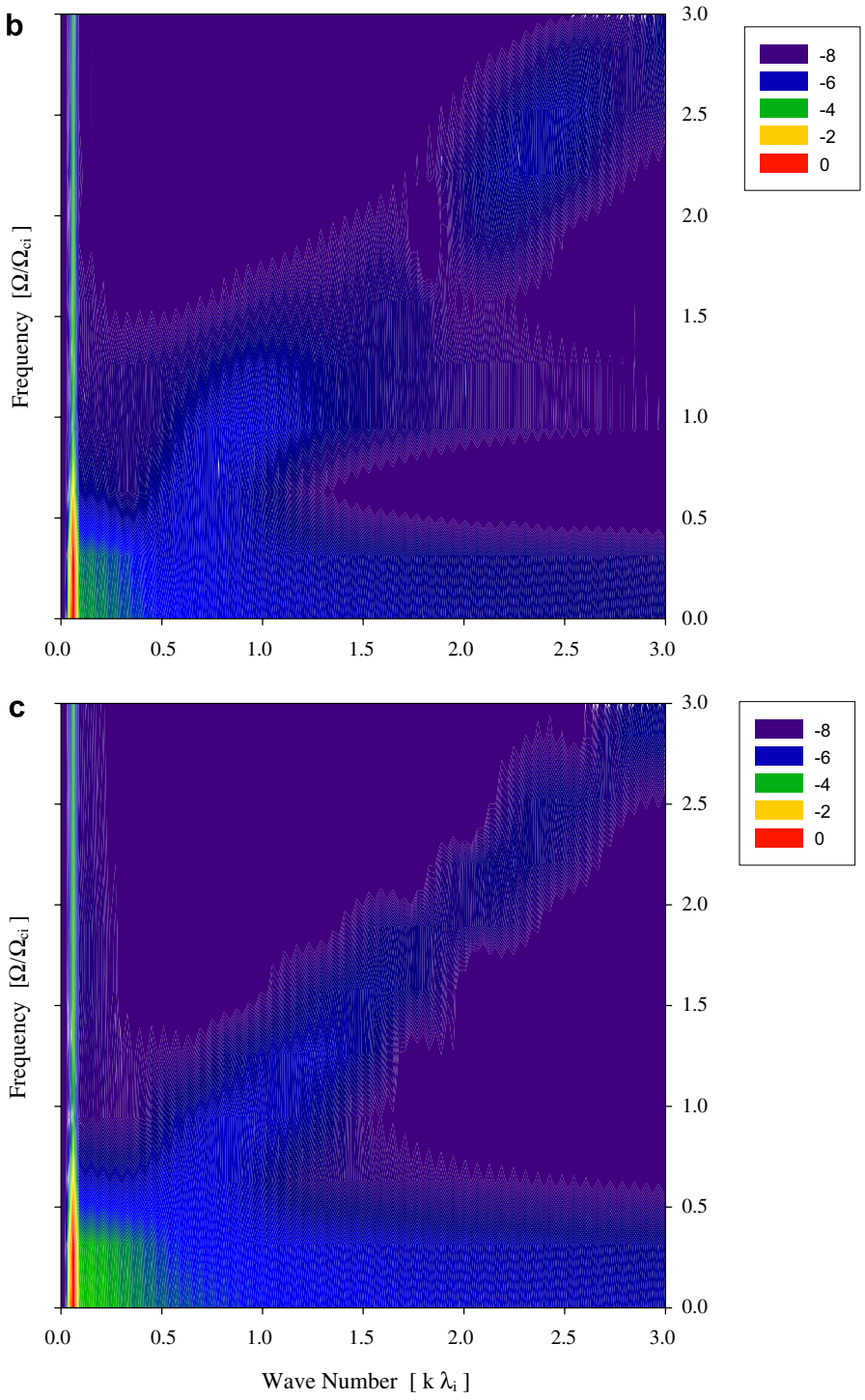

Fig. 4 (*continued*)

dispersion is observed only in PIC simulations, therefore, when the Alfvén wave propagates into PIC domain, the wave is decomposed into R- and L-mode waves. Of course, the dispersion is weak if the wave number/frequency is small enough, which is the case in the present test wave propagation with the wave-length of $\sim$105 λ_i.

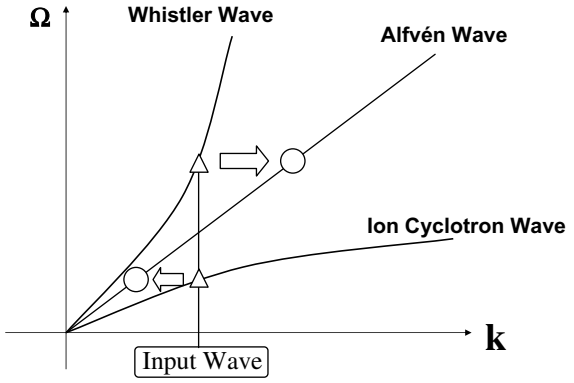

Fig. 5. The wave shift process is schematically illustrated. At the boundary between MHD and PIC domain, the waves observed in the PIC domains are shifted into the MHD mode with keeping the wave frequency.

On the other hand, in case that the wave-length is short, the Alfvén wave is decomposed into two modes in the PIC domain. The wave decomposition is schematically illustrated in Fig. 5. When the input wave is propagated from MHD to PIC domain, the wave is decomposed into Whistler wave and Ion cyclotron wave noted by triangles. Later, when these decomposed waves are ejected from PIC to MHD domain, the wave are shifted into Alfvén mode noted by circles. Resultantly, the wave form of the Alfvén waves is modified during the wave propagates in the PIC domain. This is not results from unphysical numerical error but realistic phenomena caused certainly by the kinetic effects.

Since the number of variables in MHD and PIC is different, some assumptions are necessary to connect MHD and PIC model. First, we assume that the particle velocity distribution injecting from the MHD into PIC domain is in a thermal equilibrium and it has a (shifted-) Maxwell distribution for both electrons and ions. This is because outside the PIC domain, we use the MHD model where the thermal equilibrium is generally/universally satisfied. By using the macro variables of the density, velocity, and pressure, we can set a unique (shifted-) Maxwell distribution. In addition, by using the current density with the assumption of charge neutrality, we can set the (shifted-) Maxwell distribution for both electron and ion, respectively.

The position where MHD and PIC can be connected, is a remaining issue. In case of the present Alfvén wave propagation, all the particles in PIC domain consist of thermal population, that is, in thermal equilibrium with no non-thermal particles. Therefore we can set the boundary anywhere in the MHD domain, because the thermal equilibrium is satisfied anywhere in MHD domain. We can consider that the shape of the particle velocity distribution function across the boundary is smoothly connected to the shifted-Maxwell distribution. On the other hand, in the case of that there are non-thermal particles at the boundary, the shape of the distribution function is not well continuous between PIC and MHD domains. In this case, the boundary position should be moved to an appropriate position, where the thermal equilibrium is obtained in PIC domain. For example, the shock wave creates the non-thermal particles for its dissipation process, therefore the boundary position should be far enough from the transition region to obtain the thermalized particles. For more general problems (e.g. compressional modes, multi-dimensional dynamics, and others) further investigations are necessary to find an appropriate location to connect the two different models. If the compressional mode rather than the Alfvén wave governs the dynamics, it is likely that other type of filter should be introduced in addition to the filter for $\boldsymbol{E}$ and $\boldsymbol{J}$.

Here, we have developed the new algorithm for multi-scale plasma processes called MHD and PIC interlocked simulation which is based on the domain decomposition method. The micro-domain is embedded in the macro-domain. In this algorithm, the mutual data exchange between micro and macro-models is performed across the boundary. This procedure works well in the case that the micro-domain occupies the finite size in the macro-domain. On the other hand, another type of interlocked model is possible where the characteristic scale of the microscopic process is extremely smaller than the grid size of macro-model ($R_x \sim \infty$. $R_t \sim \infty$). In the case, the results of micro-model could be reflected into the macroscopic model as some parameters on each macro-model grid. We call it as "Macro-Parameter" method instead of "Domain Decomposition" method.

For instance, if the macroscopic diffusion process is governed by the turbulence of extremely small size eddy, the microscopic simulation could be carried out to determine the diffusion coefficients in the macroscopic model. The "Macro-Parameter" method has been indeed applied recently to the MHD and PIC interlocked simulation of Magnetosphere-Ionosphere (M-I) coupling system by [5]. The boundary conditions for PIC model is given by the variables on the MHD grid. The ionization coefficient obtained from the accelerated electrons calculated in PIC model is included in the equation of the continuity in the set of MHD equations. The kinetic effect in the macroscopic MHD simulation of the M-I coupling system is reflected into the ionization process due to the precipitation of high-energy electrons into the ionosphere. Both the Domain Decomposition method and the Macro-Parameter method provide powerful ways when one implements the Macro–Micro Interlocked simulation.

In the present simulation, we have used PIC simulation as a micro-scale model. Other kinetic simulations (e.g. Vlasov model) can be also used as a micro-scale model. In the point of view of numerical noises, Vlasov model might be better than PIC model where some kinds of noises are excited because of the limited size and number of the macro-particles. As noted in Section 2.1, any short-wave-length and high-frequency waves cause the unphysical fluctuation in the MHD domain, if they propagate into the MHD domain. The noiseless model is better for the interlocked simulation, though we have introduced the low-pass filter to reduce the fluctuation excited in the PIC domain. However, even if a noiseless Vlasov model is used in the kinetic domain, the filter is necessary to reduce the power of physical high-frequency waves (e.g. Whistler wave). The power of the noises excited due to the macro-particles in the PIC model is generally quite smaller than that of the physical waves.

We have used kinetic simulation as a micro-scale model and MHD simulation as a macro-scale model. As widely known, they correspond to the two different extreme models for plasma simulations, because the MHD is applicable only for the low-frequency and long-wave-length dynamics, and the PIC model may manage any kinetics described by the Vlasov equation. On the other hand, there are several intermediate models like Hall-MHD model, two-fluid model and hybrid-simulation model, and they may be also used to construct the interlocked simulation. In those cases, different variables would have to be used to exchange the information among the models, rather than the electric field and the current density. As the scale gap is closer, the interaction is more straightforward, and more information must be shared between micro- and macro-models.

Here, we have first developed the new algorithm for the interlocking of MHD and PIC models. The macro–micro interlocked simulation is much prospective methodology for the research of multi-scale plasma processes. Magnetic reconnection, the interaction of large scale shock and particle acceleration, and the system evolution due to anomalous transports could be the important applications of the interlocked simulation. Although several subjects still remain for the practical application, the concept of "interlocking" will much extend the applicability and the potency of numerical simulations as principal tool for research and development.

Acknowledgements

The authors thank Prof. T.Sato, and the member of Holistic Simulation Research Program in the Earth Simulator Center, Japan Agency for Marine-Earth Science and Technology (JAMSTEC). This research is one of the results from the program of "Development of Multi-Scale Coupled Simulation Algorithm" in the Earth Simulator Center. This work was also supported by the Grant-in-Aid for Creative Scientific Research "The Basic Study of Space Weather Prediction" (17GS0208, Head Investigator: K. Shibata) from the Ministry of Education, Science, Sports, Technology, and Culture of Japan, and partially supported by the Grant-in-Aid for Scientific Research from Japan Society for the Promotion of Science (Scientific Research (B) 19340180).

References

[1] C.K. Birdsall, A.B. Langdon, Plasma Physics via Computer Simulation, Institute of Physics Publishing, Bristol and Philadelphia, 1985.
[2] J. Birn, E. Priest, Reconnection of Magnetic Fields: Magnetohydrodynamics and Collisionless Theory and Observations, in: J. Birn, E. Priest (Eds.), Cambridge University Press, 2007.

[3] Y. Omura, H. Matsumoto, KEMPO1 – Technical Guide to One-dimensional Electromagnetic Particle Code, in: H. Matsumoto, Y. Omura, Computer Space Plasma Physics, 1993, pp. 21–65, Terra Sci., Tokyo.
[4] T. Sato, Macro–Micro Interlocked Simulator, J. Phys. 16 (2005) 310–316.
[5] T. Sugiyama, K. Kusano, S. Hirose, A. Kageyama, MHD-PIC Connection Model in a Magnetosphere-Ionosphere Coupling System, J. Plasma Phys. 72 (6) (2006) 945–948.
[6] T. Umeda, Y. Omura, H. Matsumoto, An improved masking method for absorbing boundaries in electromagnetic particle simulations, Comput. Phys. Commun. 137 (2001) 286–299.
[7] H.S. Wijesinghe, N.G. Hadjiconstantinou, Discussion of hybrid atomistic-continuum methods for multiscale hydrodynamics, Int. J. Multiscale Comput. Eng. 2 (2004) 189–202.